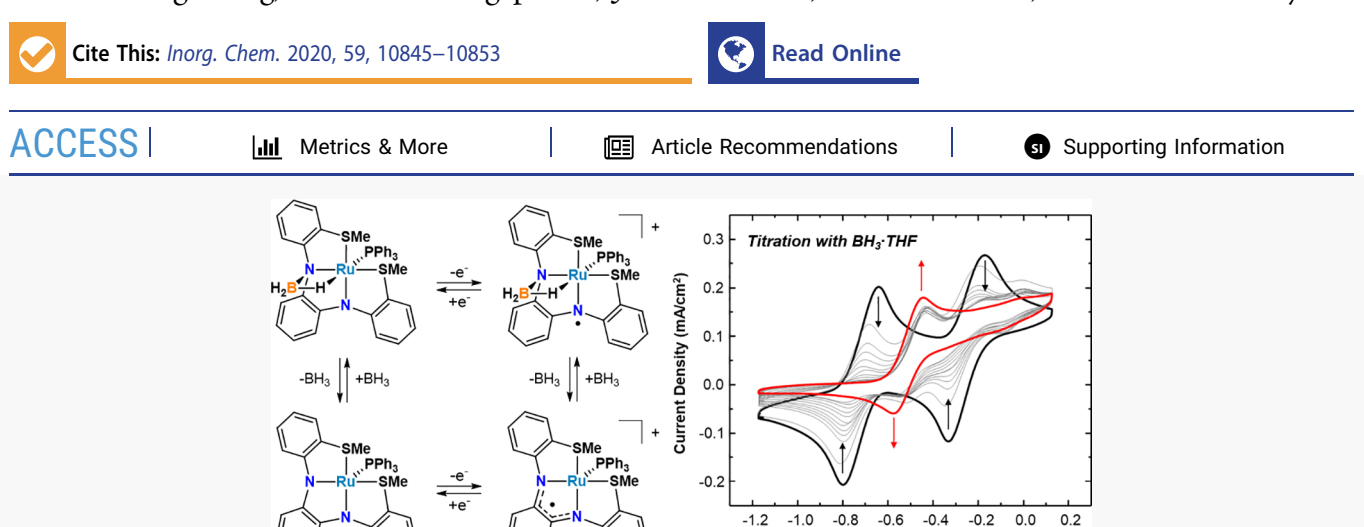
Inorganic Chemistry

Article pubs.acs.org/IC

Influence of Multisite Metal-Ligand Cooperativity on the Redox Activity of Noninnocent N2S2 Ligands

Kyle D. Spielvogel, Javier A. Luna, Sydney M. Loria, Leah P. Weisburn, Nathan C. Stumme, Mark R. Ringenberg, Gummadi Durgaprasad, Jason M. Keith,* Scott K. Shaw,* and Scott R. Daly*



ABSTRACT: Metal-ligand cooperativity (MLC) relies on chemically reactive ligands to assist metals with small-molecule binding and activation, and it has facilitated unprecedented examples of catalysis with metal complexes. Despite growing interest in combining ligand-centered chemical and redox reactions for chemical transformations, there are few studies demonstrating how chemically engaging redox active ligands in MLC affects their electrochemical properties when bound to metals. Here we report stepwise changes in the redox activity of model Ru complexes as zero, one, and two BH₃ molecules undergo MLC binding with a triaryl noninnocent N₂S₂ ligand derived from o-phenylenediamine (L1). A similar series of Ru complexes with a diaryl N₂S₂ ligand with ethylene substituted in place of phenylene (L2) is also described to evaluate the influence of the o-phenylenediamine subunit on redox activity and MLC. Cyclic voltammetry (CV) studies and density functional theory (DFT) calculations show that MLC attenuates ligand-centered redox activity in both series of complexes, but electron transfer is still achieved when only one of the two redox-active sites on the ligands is chemically engaged. The results demonstrate how incorporating more than one multifunctional reactive site could be an effective strategy for maintaining redox noninnocence in ligands that are also chemically reactive and competent for MLC.

INTRODUCTION

Metal-ligand cooperativity (MLC) is an important method for activating small molecules and accessing productive catalysis with metal complexes and metalloenzymes. Unlike reactions that take place exclusively at the metal, MLC occurs when a molecule undergoes chemical binding or heterolytic bond cleavage across the metal and an attached ligand (Scheme 1a). MLC is commonly associated with heterolytic H-H or Helement cleavage, which can occur via net 1,2-addition across a metal-ligand bond (i.e., bifunctional reactivity)² or addition across the metal and distal ligand site. MLC is also commonly observed with ambiphilic small molecules such as CO₂, isocyanates, ³ SO₂, ⁴ nitriles, ⁵ and boranes. ⁶

An emerging area of interest in catalysis has centered on the idea of combining MLC with redox-active ligands to access new synthetic transformations. While this combined reactivity has been explored in transformations with H₂⁷ and can be facilitated by proton-coupled electron transfer (PCET)⁸ and hydrogen atom transfer reactions known to occur with redox active ligands, it remains unclear as to how MLC binding with other substrates affects the electrochemical properties of metal complexes containing noninnocent ligands, especially those with multiple redox active sites. Understanding the influence MLC has on electron transfer is highly relevant to efforts aimed at combining ligand-centered chemical and redox processes for transformations with molecules other than H₂ (e.g., CO₂)¹⁰ and could be useful for evaluating reactions where both types of ligand-centered reactivity are possible.

Received: May 8, 2020 Published: July 8, 2020





Scheme 1. Metal-Ligand Cooperativity, Synthesis of 1-(BH₃), and 1-e⁻ Redox Transformations^a

a) Metal-Ligand Cooperativity (MLC) with ${\rm H_2}$ and ${\rm BH_3}$

b) Synthesis of the MLC complex 1-(BH₃)

c) One electron redox transformations with L1

 a (a) Comparison of MLC with $\rm H_2$ and BH $_3$ across M-N bonds. (b) Structures of 1 and 1-(BH $_3$). (c) 1-e $^-$ redox transformations with L1 highlighting changes from X-type amide groups to L-type imine groups.

Recently, we reported a redox-active N_2S_2 ligand derived from o-phenylenediamine that undergoes MLC binding with BH $_3$ (Scheme 1b). In the absence of MLC, the tetradentate N_2S_2 ligand L1 undergoes two successive one-electron redox processes while bound to Ni and Ru (Scheme 1c), 11,12 but the electrochemical properties have yet to be investigated when the ligand is chemically engaged in MLC.

An important distinction between engaging the nitrogen atoms in L1 using MLC compared to other means such as protonation or alkylation is that the coordination geometry of the ligand is maintained, thereby allowing the structures and electronic properties to be more directly compared to their native MLC-free complexes. In contrast, protonating the nitrogen atoms leads to structural rearrangements that change the positioning of ligand donor atoms in the metal coordination sphere. We have shown previously that protonation of 1 with HBF₄·Et₂O or benzoic acid results in a $cis-\beta$ arrangement of L1 where one of the flanking aryl groups flexes out of the equatorial plane so that the corresponding thioether and PPh₃ ligand swap places (Scheme 2).¹¹ Under these circumstances, it would be difficult to delineate between electronic structure changes that arise due to chemical engagement at N and those that arise due to ligand rearrangement in the inner coordination sphere.

Here we report how MLC binding in Ru complexes affects the electrochemical properties of redox active L1 upon chemical engagement of one and then both of the nitrogen atoms. We also report redox reactions with MLC-bound BH₃ in a related series of Ru complexes that contain a tetradentate

Scheme 2. Reaction of 1 with Benzoic Acid

 N_2S_2 ligand with ethylene in place of the phenylene backbone (L2; Chart 1).

Chart 1. L1 and L2 and General Labeling Scheme for Bond Distances in Table 1

RESULTS AND DISCUSSION

Synthesis and Characterization. We previously reported the synthesis of 1 and 1-(BH₃), 11 as shown in Scheme 1b, and here we report synthesis of 2 and 2-(BH₃) for comparison (Chart 1). As described previously for 1, the formally 16-electron Ru complex 2 was prepared by treating RuCl₂(PPh₃)₃ with H₂(L2) and 2 equiv of NaO'Bu (Scheme 3). Once crystallized, 2 was treated with BH₃·THF in THF to form an 18-electron MLC compound 2-(BH₃).

Scheme 3. Synthesis of 2 and 2-(BH₃)

XRD studies confirmed BH3 binding across one of the Ru-N bonds with L2 and allowed the structures of 2 and 2-(BH₃) to be compared (Figure 1). As with 1, the Ru-N bonds in 2 are relatively short at 1.990(2) and 2.006(1) Å due to the π donor properties of the amido groups (Table 1). Engagement of the N lone pair in MLC binding attenuates N \rightarrow Ru π donation and causes the Ru-N bond to elongate from 2.006(1) Å in 2 to 2.076(3) in 2-(BH₃). MLC also causes the N2-C2 and N2-C21 bond distances in 2 to increase from 1.463(3) and 1.355(2) Å, respectively, to 1.495(4) and 1.443(5) in 2-(BH₃). The N-B distance in 2-(BH₃) is shorter in 1-(BH₃) (1.558(6) and 1.611(7) Å, respectively), which suggests increased Lewis basicity of the less conjugated amido groups in L2 compared to L1. MLC also has a significant influence on the Ru-P bond distance, which increases from 2.1949(6) Å in 2 to 2.322(1) Å in 2-(BH₃) due to hydride occupation in the open coordination site trans to PPh3.

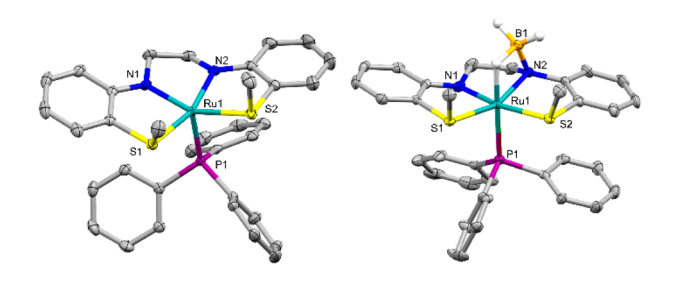


Figure 1. Molecular structures of 2 (left) and $2-(BH_3)$ (right). Thermal ellipsoids are drawn at the 50% level. Hydrogen atoms attached to carbon were omitted from the figure.

Table 1. Select Bond Distances (Å) from Single-Crystal XRD Data

	1^a	$1-(BH_3)^a$	$1-(BH_3)_2$	[1-MeCN]BF ₄	1-Cl ₂	2	2-(BH ₃)	$[2-(BH_2)]OTf$
Ru-N1	2.008(6)	2.039(4)	2.0840(17)	2.022(2)	1.968(4)	1.990(2)	2.039(3)	2.098(2)
Ru-N2	2.009(6)	2.097(4)	2.0839(17)	2.015(2)	1.972(4)	2.006(1)	2.076(3)	2.094(1)
Ru-S1	2.329(2)	2.327(1)	2.3031(6)	2.3502(7)	2.370(1)	2.3426(5)	2.329(1)	2.3283(5)
Ru-S2	2.322(2)	2.316(1)	2.3031(6)	2.3416(7)	2.374(2)	2.3215(6)	2.337(1)	2.3223(5)
Ru-P	2.196(2)	2.317(1)		2.3121(7)		2.1949(6)	2.322(1)	2.3012(4)
Ru-L ^b		1.77(4)	1.68(2)	2.119(2)	2.373(1)		1.70(3)	1.80(2)
Ku-L			1.68(2)		2.379(1)			
C1-C2	1.453(10)	1.449(4)	1.407(4)	1.438(4)	1.455(8)	1.522(3)	1.535(5)	1.547(2)
N1-C1	1.39(1)	1.385(5)	1.462(3)	1.376(3)	1.351(6)	1.470(2)	1.455(5)	1.493(2)
N2-C2	1.39(1)	1.465(6)	1.462(3)	1.376(3)	1.360(7)	1.463(3)	1.495(4)	1.490(2)
N1-C11	1.39(1)	1.374(6)	1.463(3)	1.393(3)	1.426(6)	1.363(2)	1.344(5)	1.443(2)
N2-C21	1.41(1)	1.452(6)	1.463(3)	1.398(3)	1.425(5)	1.355(2)	1.443(5)	1.438(2)
NI D		1.611(7)	1.567(3)				1.558(6)	1.557(2)
N-B								1.561(2)

^aData reported previously in ref 11. ^bL corresponds to Cl, H, or MeCN.

NMR and IR spectroscopy were used to further confirm the presence of MLC binding in 2-(BH₃). The ³¹P NMR resonance for 2 at δ 89.24 ppm shifts to higher field (δ 44.34 ppm) and splits into a doublet for 2-(BH₃) in CD₂Cl₂ due to trans P-Ru-H coupling (J = 50 Hz). A broad Ru-H-B hydride resonance also appeared in the ¹H NMR spectrum at δ -7.96 ppm in CD₂Cl₂, and trans P-Ru-H coupling was more clearly observed in C₆D₆ (Figure S16). The terminal B-H resonances yielded a very broad resonance with a full width at half-maximum (fwhm) of 470 Hz centered at δ 1.22 ppm. The 11B NMR spectrum in CD2Cl2 also revealed a broad resonance at $\delta - 18.3$ ppm with no clear $^{11}B-^{1}H$ coupling, but the solid-state IR spectra of 2-(BH₃) showed distinct bridging and terminal B-H stretches at 2346, 2417, and 2432 cm⁻¹, respectively. These are similar to B-H stretches reported for 1-(BH₃) at 2338 cm⁻¹ (B-H-Ru) and 2404 and 2430 cm⁻¹ (terminal B-H).¹¹

Dual-MLC compound 1-(BH₃)₂ was prepared by refluxing RuCl₃·xH₂O with L1 and EtOH in air to form 1-Cl₂, followed by reduction of 1-Cl₂ with 2 equiv of NaBH₄ (Figure 2a). Structures of 1-Cl₂ and 1-(BH₃)₂ obtained from single-crystal XRD studies revealed C_s and C_2 symmetry, respectively, with chlorides and hydrides bound in the axial coordination sites. Evaluating the two structures side-by-side revealed changes indicative of redox processes involving L1. The ligand bond distances in 1-Cl₂ suggest that the o-phenylenediamine was oxidized to the neutral diiminoquinone; the short N-C bond distances of 1.351(6) and 1.360(7) Å are consistent with significant double-bond character. In contrast, the N-C distances in the structure of 1-(BH₃)₂ are elongated to 1.462(3) Å. Furthermore, the NC-CN distance decreased from 1.455(8) Å in 1-Cl₂ to 1.407(4) Å in 1-(BH₃)₂ consistent with reduction of the diiminoquinone back to o-phenylenediamine. The N-B distances shortened from 1.611(7) Å in 1- (BH_3) to 1.567(3) Å in 1- $(BH_3)_2$.

The ¹H NMR spectrum for 1-Cl₂ revealed that the complex is diamagnetic and showed chemically equivalent SMe resonances consistent with the symmetric structure (Figure S9). In contrast, three sets of SMe and hydride resonances were observed in the ¹H NMR spectrum of 1-(BH₃)₂ consistent with three different stereoisomers, as shown in Chart 2. The hydride ¹H resonances were broad at RT but became more resolved upon cooling to -80 °C (Figure 3).

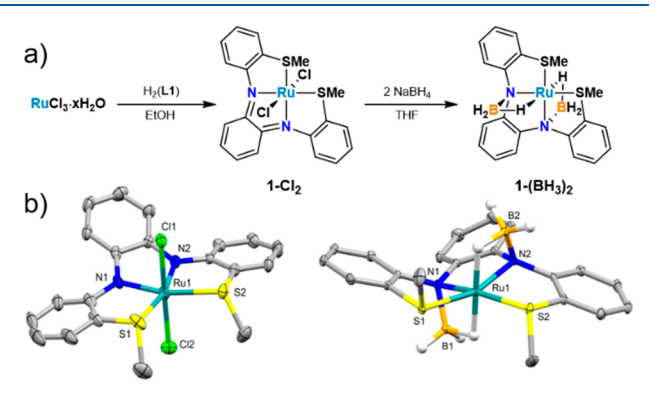
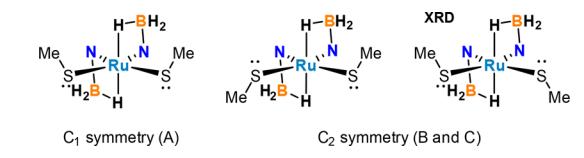


Figure 2. (a) Synthesis of 1-Cl_2 and $1\text{-}(BH_3)_2$. (b) Molecular structures of 1-Cl_2 (left) and $1\text{-}(BH_3)_2$ (right). Thermal ellipsoids are drawn at the 50% level. Hydrogen atoms attached to carbon were omitted from the figure.

Chart 2. Comparison of Stereoisomers A, B, and C of 1- $(BH_3)_2$



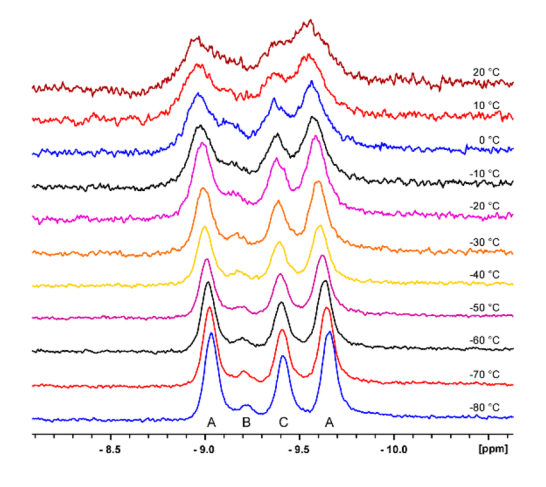


Figure 3. Variable-temperature 1H NMR studies (hydride region) of $1-(BH_3)_2$ in CD_2Cl_2 .

Isomer A has two inequivalent hydride resonances that appear at δ -9.03 and -9.67 ppm, whereas the C_2 symmetric isomers B and C have chemically equivalent hydrides that generate a single resonance for each isomer at δ -9.22 and -9.42 ppm (we cannot distinguish between the resonances for B and C, but we suspect that the XRD isomer C is in higher abundance). The relative intensities of the hydride resonances align with three sets of SMe resonances at -80 °C (δ 2.88 and 2.64 ppm (A), δ 2.70 ppm (B), and δ 2.94 ppm (C)), suggesting that they originate from the same diastereomers (Figure S13). Similar to 2-(BH₃), a broad ¹H resonance assigned to the terminal B-H bonds was observed at δ 1.72 ppm (fwhm = 280 Hz) and became more resolved at lower temperature. The room-temperature ¹¹B NMR spectrum revealed a single resonance at δ -9.3 ppm, and this peak broadened as the sample was cooled (Figure S12). Similar to 1-(BH₃) and 2-(BH₃), the IR spectrum of 1-(BH₃), revealed bridging B-H-Ru stretches at 2336 cm⁻¹ and terminal B-H stretches at 2411 and 2435 cm⁻¹.

Electrochemical Studies. Cyclic voltammetry (CV) data were collected to determine how MLC binding affects the electrochemistry of 1 and 2 and to evaluate the importance of the *o*-phenylendiamine subunit for redox chemistry (Table 2).

Table 2. CV Data Referenced to Fc/Fc^+ and Collected at 100 mV/s

	$E_{1/2}$ (V)	$E_{\rm pa}-E_{\rm pc}$ (V)	$I_{\rm pc}/I_{\rm pa}$
1	-0.72	0.16	0.975
	-0.25	0.16	0.954
1-(BH ₃)	-0.50	0.13	0.617
2	-1.00	0.11	0.924
	-0.62	0.15	0.777
	-0.21	0.15	0.922
2-(BH ₃)	-0.72	0.13	0.984

As reported previously but recapped here for comparison, ¹¹ the CV of **1** shows two reversible waves at $E_{1/2} = -0.72$ V ($I_{\rm pc}/I_{\rm pa} = 0.975$)¹³ and $E_{1/2} = -0.25$ V ($I_{\rm pc}/I_{\rm pa} = 0.954$) vs the Fc/Fc⁺ couple, ¹⁴ the internal standard for all potentials reported herein. Consistent with the assignment of similar CV features for Ni complexes with L1, ¹² the first reversible wave at -0.72 V is assigned as the $1^+/1$ couple, and the second wave at -0.25 V is assigned as the $1^{2+}/1^+$ couple. ¹⁵

Unexpectedly, our initial attempts to collect the CV of 1-(BH₃) in THF revealed three reversible features instead of two observed for 1 under the same conditions (Figure 4). The results were qualitatively the same when CV data were collected in MeCN under the same conditions (Figure S2). All three waves for 1-(BH₃) were present during initial scans collected at different starting potentials, which ruled out that the additional feature was due to an ECE-type mechanism. Furthermore, no scan-to-scan decomposition was observed for multiple samples collected over 100s of scans (Figure S4).

A clue as to the origin of the three features in the CV of 1- (BH_3) was afforded by replicate analysis in THF and MeCN. The current density of the middle feature at -0.50 V varied slightly from sample-to-sample and was inversely related to the current density of the two flanking features at -0.72 and -0.25 V. Suspecting that the three CV features represented an equilibrium mixture of 1 and 1- (BH_3) , we performed a titration study maintaining the concentration of 1 and adding BH_3 . THF (which shows no redox activity in our electro-

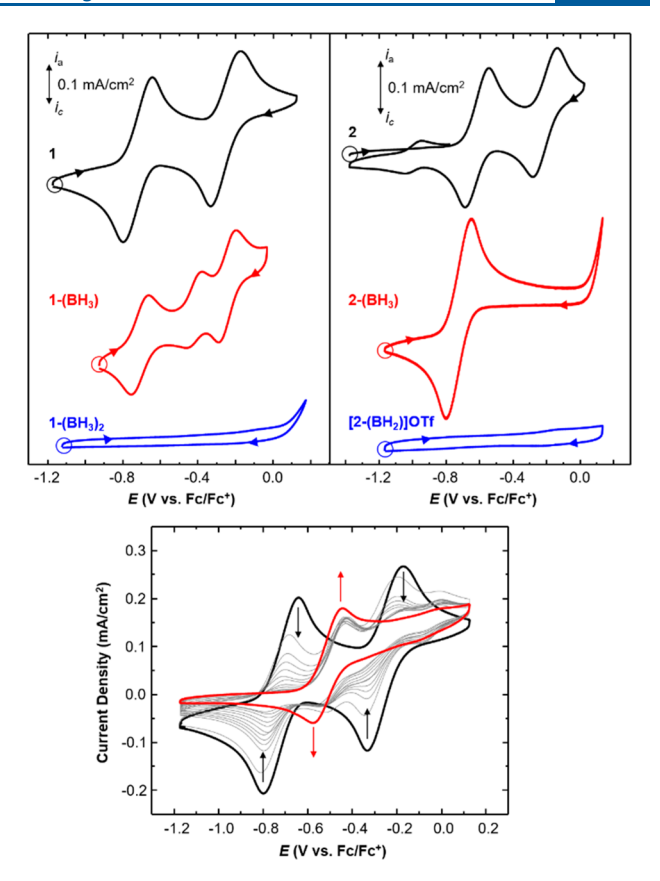


Figure 4. Top: CVs of 1 (left) and 2 (right) collected at 100 mv/s with and without MLC as indicated. Scan starting potentials are circled, and scan directions are indicated with arrows. Bottom: Titration of 1 (black trace) by addition of BH $_3$ ·THF. The gray traces show addition of BH $_3$ ·THF in 0.1 M increments up to 1.5 equivalents. The red trace shows the CV with a large excess (5.5 equiv) of BH $_3$ ·THF. All CV data were collected in THF with 0.1 M ("Bu $_4$ N)PF $_6$ using a glassy carbon working electrode, Pt wire counter electrode, and Pt wire quasi-reference electrode. Potentials are normalized to the Fc/Fc $^+$ redox couple.

chemical window). Indeed, CV data acquired after each addition show the gradual disappearance of the two features assigned to 1 and an increase in current density for a new, single feature that appeared at $-0.50 \text{ V } (I_{\rm pc}/I_{\rm pa}=0.617)$ after addition of excess BH₃·THF (Figure 4 bottom).

CV data collected on different ratios of 1 and BH₃·THF helped reveal the cause of the sample-to-sample differences observed in replicate CVs of crystallized 1-(BH₃). Solid samples of 1-(BH₃) appear to lose various amounts of BH₃ when exposed to vacuum for extended periods, which occurred when transferring different samples under vacuum to our analytical glovebox for electrochemical analysis. The CV of 1-(BH₃) in Figure 4, for example, has a profile and peak intensities more closely matched to the CV we obtained for 1 with 0.5 equiv of BH₃·THF (Figure S5). For comparison, the CV of 1 with 1.0 mol equiv of BH₃·THF shows that both 1-(BH₃) and 1 exist in equilibrium in a 5:1 molar ratio (Figure S6)

The equilibrium observed by CV between 1 and 1-(BH₃) was initially unexpected because NMR data collected on crystals of 1-(BH₃) immediately isolated from their mother liquor showed no obvious evidence of 1 and free BH₃·THF in C_6D_6 and THF- d_8 . However, these spectroscopic and electrochemical differences can likely be attributed to changes

in BH₃ lability when **1-(BH₃)** is oxidized under an applied potential. As shown in Scheme 4, BH₃ can be lost from **1-(BH₃)** in THF to form BH₃·THF before or after oxidation. We postulated that oxidized **1-(BH₃)** loses BH₃ more readily because this allows the ligand radical to delocalize over both nitrogen atoms and more of the triaryl framework. Indeed, DFT calculations (methods described in the "DFT Calculations" section) support this hypothesis, and they were used to calculate ΔG values for the following two equilibrium expressions:

$$\mathbf{1} + \mathrm{BH_3 \cdot THF} \rightleftharpoons \mathbf{1 \cdot (BH_3)} + \mathrm{THF}$$

$$\Delta G_1 = -7.5 \text{ kcal/mol} \tag{1}$$

$$\mathbf{1}^+ + \mathrm{BH_3 \cdot THF} \rightleftharpoons \mathbf{1 \cdot (BH_3)^+} + \mathrm{THF}$$

 $\Delta G_2 = -5.5 \text{ kcal/mol}$ (2)

The calculations show that BH_3 binding is less favorable by 2.0 kcal/mol when 1 is oxidized.

Scheme 4. Electron and BH_3 Transfer Series with 1 and 1- (BH_3)

We modeled the experimental titration data for comparison to the calculated ΔG values. Because we cannot discern between the two different equilibria afforded by neutral and oxidized 1 in the CV data, we used a single net equilibrium expression that simply accounts for total concentration of 1 and 1-(BH_3) based on peak currents and as a function of added BH₃·THF (see the Supporting Information for details). The experimental model yielded a net $\Delta G = -6.4 \pm 0.4$ kcal/mol, in excellent agreement with the calculated data. These calculated and experimental ΔG values compare very well with energies reported for formation of Lewis acid—base adducts between amines and BH₃. 16

Given that MLC binding in 1-(BH₃) eliminated one of the redox features observed in the CV of 1, we tested dual-MLC compound 1-(BH₃)₂ for comparison. Consistent with the CV results for 1-(BH₃), the redox activity in 1-(BH₃)₂ is completely attenuated due to MLC engagement of both N atoms (Figure 4). No evidence of BH₃ loss was observed for 1-(BH₃)₂ under an applied potential.

We recently showed that replacing o-phenylenediamine in L1 with nonconjugated 1,2-diaminoethane in L2 significantly attenuates reversible redox activity in square planar Ni complexes. In contrast, the CV of 2 maintains quasi-reversible and reversible redox features at -0.62 V ($I_{\rm pc}/I_{\rm pa}=0.777$) and -0.21 V ($I_{\rm pc}/I_{\rm pa}=0.922$), respectively. A new, relatively small, reversible feature ($I_{\rm pc}/I_{\rm pa}=0.924$) emerged in

the CV trace of 2 at -1.00 V, which is assigned to an ECE process and a new electrochemically generated complex that has yet to be identified. This ECE feature is only observed for 2 when scanning past the most positive oxidation event at -0.21 V.

The CV of $2\text{-}(BH_3)$ again showed how MLC reduces the electrochemical activity of 2; a single, reversible redox wave was observed at -0.72 V ($I_{pc}/I_{pa}=0.984$). There was no evidence of an equilibrium between $2\text{-}(BH_3)$ and 2 (i.e., bound and unbound BH_3) as observed for $1\text{-}(BH_3)$, which suggests that MLC binding is stronger in $2\text{-}(BH_3)$ than $1\text{-}(BH_3)$. The increased MLC binding strength is consistent with the shorter N–B bond length of 1.558(6) Å for $2\text{-}(BH_3)$ relative to the 1.611(7) Å length for $1\text{-}(BH_3)$.

To compare BH_3 binding energies between 1 and 2, we again used DFT to calculate the change in Gibbs free energy for the reaction of 2 and 2^+ with BH_3 . THF:

2 + BH₃·THF
$$\rightleftharpoons$$
 2-(BH₃) + THF

$$\Delta G_3 = -15.2 \text{ kcal/mol}$$
(3)

$$2^+ + BH_3$$
·THF $\rightleftharpoons 2$ - $(BH_3)^+ + THF$
 $\Delta G_4 = -15.2 \text{ kcal/mol}$ (4)

The results show that BH_3 binding with 2 is significantly more exergonic than that with 1, which aligns with differences in the CVs of 1-(BH_3) and 2-(BH_3) and their B-N bond distances. Furthermore, in contrast to our calculations with 1, the binding energies are the same regardless if 2 is neutral or oxidized. This result lends support to our hypothesis that the 2.0 kcal difference in the ΔG of reaction for 1 and 1⁺ (eqs 1 and 2) can be attributed to additional stabilization afforded by the conjugated phenylene backbone in 1⁺, which allows the radical to delocalize over both N positions when BH_3 is lost.

Chemical Oxidation Studies. Chemical oxidation studies were carried out to identify the electrochemically generated complexes in the CV traces. Treating 1 with AgBF₄ in MeCN afforded the singly oxidized complex [1-MeCN]BF₄ (Scheme 5). XRD studies revealed MeCN bound in the open

Scheme 5. Chemical Oxidation of 1 to Form [1-MeCN]BF₄

coordination site trans to PPh₃ and the presence of the outer-sphere BF₄⁻ (Figure S8). Only subtle changes to the C–C and C–N bond distances on the ligand were observed compared to those of 1 (Table 1), which suggested a high degree of radical delocalization over the ligand metal. EPR data collected on frozen CH₂Cl₂ solutions of [1-MeCN]BF₄ at 4 K confirmed the presence of the radical with significant electron spin delocalized across Ru and the N₂S₂ ligand (Figure 5). The EPR spectrum was modeled as an S=1/2 system with g=2.0057 and $A^{Ru}=74$ MHz. The g value is close to that of a free electron, as expected for a ligand-centered radical, but the A^{Ru} value suggests there is a non-negligible ruthenium component. For comparison, typical g-values for Ru(III) can range from

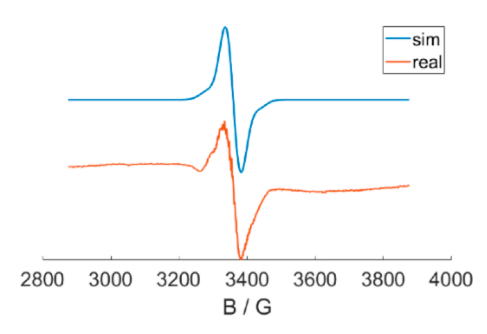


Figure 5. Frozen-solution EPR spectra of [1-MeCN]BF₄ in CH₂Cl₂ at 4 K in the X-band (9.5 MHz) were recorded with a Bruker EMX System. Fitting parameters: LW 5.5, g = 2.0057, and $A^{Ru} = 74$ MHz. Simulations were performed using the EasySpin V5.2.28 package for Matlah

2.033 to 2.205¹⁷ and would show the expected rhombohedral signal for a metal based radical, as is the case with open-shell metal systems at 4 K.¹⁸ No other hyperfine interactions could be determined due to line broadening.

Attempts to chemically oxidize 1 in THF instead of MeCN resulted in mixtures that produced poorly diffracting crystals showing evidence of ligand decomposition via C–S bond cleavage. In contrast to MeCN, we have shown previously that THF does not bind to the open coordination site trans to PPh₃ in 1.¹¹ Although 1 is stable with respect to decomposition on the time scale of the CV experiments in THF, it appears that donor molecules that bind more readily to the open coordination site in 1⁺ (such as MeCN) are required to prevent eventual decomposition after chemical oxidation.

As with 1, chemical oxidation of 2 and 1-(BH₃) with silver salts revealed immediate color changes and precipitation of a solid presumed to be Ag(0), but attempts to isolate products from the reaction mixtures were unsuccessful. We suspect that these attempts were thwarted by complications associated with the lability of BH₃ with 1 in solution and ECE transformations for 2, as observed in their CVs. In contrast, we discovered that treating 2-(BH₃) with AgOTf in THF yielded a new product that could be isolated reproducibly as single crystals in moderate yields (40–60%). XRD analysis of the single crystals from toluene revealed that MLC-bound BH₃ lost a hydride to form [2-(BH₂)]OTf with symmetric BH₂ bridged between the N atoms (Figure 6).¹⁹

NMR studies revealed that [2-(BH₂)]OTf is diamagnetic, and the complex can be formally described as Ru(II) with an anionic dihydroborate ligand and an outer-sphere triflate to balance the charge. 1H NMR data revealed the presence of chemically equivalent SMe and ethylene resonances (Figure S19). A broad hydride resonance was observed at δ –5.49 ppm, and the ^{31}P NMR spectrum revealed a doublet at δ 52.83 ppm with similar trans P–Ru–H coupling as 2-(BH₃) (J = 65 Hz). CV studies of [2-(BH₂)]OTf in THF revealed no electrochemical activity (Figure 4). This result is again attributed to MLC engagement of both N atoms on the N_2S_2 ligand, as observed for 1-(BH₃)₂.

It has been shown previously that N radicals generated by N-H hydrogen atom abstraction from $MeNH_2 \rightarrow BH_3$ react with coordinated BH_3^{20} as shown in eq 5:

$$\text{MeNH}_2 \rightarrow \text{BH}_3 \xrightarrow[-^t\text{BuO+}]{^t\text{BuO+}} \text{MeNH} \rightarrow \text{BH}_3 \xrightarrow[-1/2\text{H}_2]{} \text{MeNH-BH}_2$$

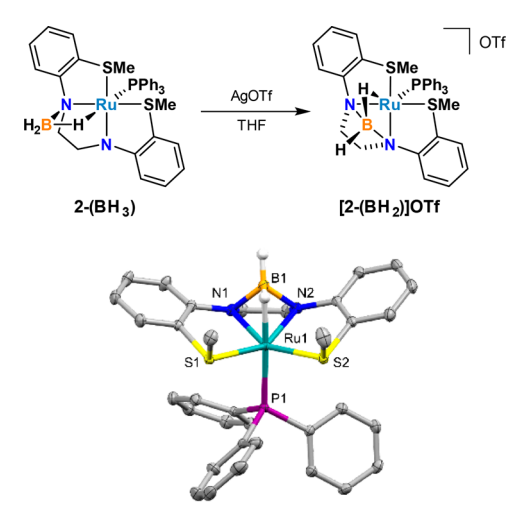


Figure 6. (Top) Reaction of $2-(BH_3)$ with AgOTf. (Bottom) Molecular structures of $[2-(BH_2)]$ OTf. Thermal ellipsoids are drawn at the 50% level. Hydrogen atoms attached to carbon and the triflate anion were omitted from the figure.

It is plausible that similar N radical reactivity is operative when **2-(BH₃)** is oxidized, although we have yet to confirm that a stochiometric amount of H₂ is generated in this reaction. Furthermore, it is possible that AgOTf reacts directly with MLC-bound BH₃ rather than oxidizing the ligand first. Control reactions without **2-(BH₃)**, for example, showed that AgOTf reacts with BH₃·THF in THF to form a precipitate and new ¹¹B NMR resonances similar to those reported for Lewis base adducts of H₂B-OTf (Figure S22).²¹ Efforts to elucidate the mechanism of this reaction are ongoing.

DFT Calculations. Given the difficulties isolating singly oxidized 1-(BH₃)⁺, 2⁺, and 2-(BH₃)⁺ for experimental analysis, dispersion-corrected DFT calculations (B3LYP-d3)²² were conducted using Gaussian²³ to evaluate the influence of MLC on spin densities and to calculate changes in Gibbs free energies upon BH₃ binding (as described above). Calculations on neutral and oxidized 1 and 2 with and without BH₃ and on [1-MeCN]⁺ were performed for comparison to the experimental results. The calculated bond distances, which are summarized in Table S5, reproduce the relative bond distance variations observed in the experimentally determined structures.²⁴

The DFT calculations suggest significant spin delocalization across the covalent Ru–N bonds for all of the oxidized complexes, consistent with the noninnocent character of the N_2S_2 ligands. Mulliken spin densities calculated for [1-MeCN]⁺ with coordinated MeCN were 13.9% for Ru and 45.2% for N atoms on L1 (Table 3), with the remaining spin being delocalized over the rest of the triaryl framework (Table S2). These values are consistent with the EPR results showing

Table 3. Calculated Mulliken Spin Densities for Ru and N^a

	Ru	N1	N2	total N
[1-MeCN] ⁺	13.9%	22.8%	22.4%	45.2%
1+	27.4%	19.0%	17.5%	36.5%
1-(BH ₃)+	22.7%	41.5%	0.1%	41.6%
2+	27.7%	21.3%	28.9%	50.2%
2-(BH ₃) ⁺	32.9%	45.1%	-0.6%	44.5%

^aThe full list of values can be found in the Supporting Information.

(5)

mostly ligand-centered radical character for [1-MeCN]BF₄. Removing the coordinated MeCN to form five-coordinate 1^+ shifts more spin density onto Ru (27.4%) with a corresponding decrease on the ligand N atoms (36.5%). Similar results were obtained for 2^+ without MeCN, albeit with more spin density located on N (50.2%) due to the absence of the conjugated o-phenylenediamine subunit (Tables 3 and S3).

Side-by-side spin density plots for oxidized 1^+ and 2^+ with and without BH₃ clearly shows how MLC binding in $1-(BH_3)^+$ and $2-(BH_3)^+$ eliminates spin density on the chemically engaged N atom and prevents π delocalization with the associated flanking aryl group (Figure 7). The N spin densities

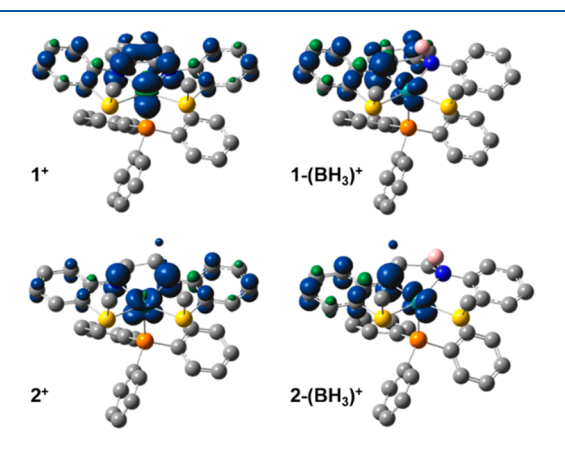


Figure 7. Calculated spin density plots of singly oxidized complexes. Hydrogen atoms were omitted from the figure. Isovalues are shown at 0.004, and associated spin density values are shown in Table 2.

in $1-(BH_3)^+$ (41.6%) and $2-(BH_3)^+$ (44.5%) are similar to those calculated for their parent complexes, 1^+ and 2^+ , but have shifted to the unoccupied N atoms (Table 3). These data visually demonstrate how N atoms are not available for ligand-centered redox transformations when engaged in MLC with BH₃, supporting our experimental data and assignments of redox (in)activity.

CONCLUSION

In summary, we have shown how stepwise MLC engagement of amido groups in redox active N₂S₂ ligands attenuates their electrochemical reactivity when bound to Ru. Although the results are somewhat intuitive when considering how MLC chemically removes part of the π -surface accessible for ligandcentered oxidation, they demonstrate how electron transfer can still be achieved as long as a redox-active site remains available and unoccupied. This suggests that combining MLC with redox active ligands may be more productive for accessing new synthetic transformations if more than one multifunctional reactive site is incorporated into the ligand (as shown here) or if chemical and redox-active functional groups on the ligands are separated. The results also serve as a reminder that chemical-induced attenuation of ligand-centered redox activity should be accounted for when evaluating reaction mechanisms that invoke chemical and redox processes at the same noninnocent ligand.

ASSOCIATED CONTENT

Supporting Information

The Supporting Information is available free of charge at https://pubs.acs.org/doi/10.1021/acs.inorgchem.0c01353.

Tabulated crystallographic data, experimental and calculated bond distances, Mulliken charges and spin density, spectra, and experimental details(PDF)

Coordinates of calculated structures(XYZ)

Accession Codes

CCDC 1988544–1988549 contain the supplementary crystallographic data for this paper. These data can be obtained free of charge via www.ccdc.cam.ac.uk/data_request/cif, or by emailing data_request@ccdc.cam.ac.uk, or by contacting The Cambridge Crystallographic Data Centre, 12 Union Road, Cambridge CB2 1EZ, UK; fax: +44 1223 336033.

AUTHOR INFORMATION

Corresponding Authors

Jason M. Keith — Department of Chemistry, Colgate University, Hamilton, New York 13346, United States; o orcid.org/0000-0002-5292-397X; Email: jkeith@colgate.edu

Scott K. Shaw — Department of Chemistry, The University of Iowa, Iowa City, Iowa 52242, United States; orcid.org/0000-0003-3767-3236; Email: scott-k-shaw@uiowa.edu

Scott R. Daly — Department of Chemistry, The University of Iowa, Iowa City, Iowa 52242, United States; o orcid.org/0000-0001-6229-0822; Email: scott-daly@uiowa.edu

Authors

Kyle D. Spielvogel – Department of Chemistry, The University of Iowa, Iowa City, Iowa 52242, United States

Javier A. Luna — Department of Chemistry, The University of Iowa, Iowa City, Iowa 52242, United States

Sydney M. Loria – Department of Chemistry, Colgate University, Hamilton, New York 13346, United States

Leah P. Weisburn – Department of Chemistry, Colgate University, Hamilton, New York 13346, United States

Nathan C. Stumme – Department of Chemistry, The University of Iowa, Iowa City, Iowa 52242, United States

Mark R. Ringenberg — Universität Stuttgart, Institut für Anorganische Chemie, 70569 Stuttgart, Germany; orcid.org/0000-0001-7585-5757

Gummadi Durgaprasad — Department of Chemistry, The University of Iowa, Iowa City, Iowa 52242, United States

Complete contact information is available at: https://pubs.acs.org/10.1021/acs.inorgchem.0c01353

Author Contributions

*K.D.S. and J.A.L. contributed equally to this work.

Notes

The authors declare no competing financial interest.

ACKNOWLEDGMENTS

This work was generously supported by the National Science Foundation (1650894 and 1651381). We thank Dale Swenson for collecting the single-crystal XRD data. We thank Johna Leddy for her assistance in developing a model for the CV titration data.

REFERENCES

(1) (a) Khusnutdinova, J. R.; Milstein, D. Metal-Ligand Cooperation. *Angew. Chem., Int. Ed.* **2015**, *54*, 12236–12273. (b) Gruetzmacher, H. Cooperating ligands in catalysis. *Angew. Chem., Int. Ed.* **2008**, *47*, 1814–1818. (c) van der Vlugt, J. I.; Reek, J. N. H. Neutral Tridentate PNP Ligands and Their Hybrid Analogs: Versatile Non-Innocent Scaffolds for Homogeneous Catalysis. *Angew. Chem., Int. Ed.*

2009, 48, 8832-8846. (d) Feichtner, K.-S.; Gessner, V. H. Cooperative bond activation reactions with carbene complexes. Chem. Commun. 2018, 54, 6540-6553. (e) Omann, L.; Koenigs, C. D. F.; Klare, H. F. T.; Oestreich, M. Cooperative Catalysis at Metal-Sulfur Bonds. Acc. Chem. Res. 2017, 50, 1258-1269. (f) Verhoeven, D. G. A.; Moret, M.-E. Metal-ligand cooperation at tethered π -ligands. Dalton Trans. 2016, 45, 15762-15778. (g) Higashi, T.; Kusumoto, S.; Nozaki, K. Cleavage of Si-H, B-H, and C-H Bonds by Metal-Ligand Cooperation. Chem. Rev. 2019, 119, 10393-10402. (h) Li, H.; Goncalves, T. P.; Lupp, D.; Huang, K.-W. PN3(P)-Pincer Complexes: Cooperative Catalysis and Beyond. ACS Catal. 2019, 9, 1619-1629. (i) Habraken, E. R. M.; Jupp, A. R.; Brands, M. B.; Nieger, M.; Ehlers, A. W.; Slootweg, J. C. Parallels between Metal-Ligand Cooperativity and Frustrated Lewis Pairs. Eur. J. Inorg. Chem. 2019, 2019, 2436-2442. (j) van der Vlugt, J. I. Cooperative Catalysis with First-Row Late Transition Metals. Eur. J. Inorg. Chem. 2012, 2012, 363-375. (k) Kuwata, S.; Ikariya, T. Metal-ligand bifunctional reactivity and catalysis of protic N-heterocyclic carbene and pyrazole complexes featuring β -NH units. Chem. Commun. **2014**, 50, 14290–14300.

- (2) (a) Morris, R. H. Exploiting Metal-Ligand Bifunctional Reactions in the Design of Iron Asymmetric Hydrogenation Catalysts. *Acc. Chem. Res.* **2015**, *48*, 1494–1502. (b) Dub, P. A.; Gordon, J. C. The mechanism of enantioselective ketone reduction with Noyori and Noyori-Ikariya bifunctional catalysts. *Dalton Trans.* **2016**, *45*, 6756–6781.
- (3) (a) Stichauer, R.; Helmers, A.; Bremer, J.; Rohdenburg, M.; Wark, A.; Lork, E.; Vogt, M. Rhenium(I) Triscarbonyl Complexes with Redox-Active Amino- and Iminopyridine Ligands: Metal-Ligand Cooperation as Trigger for the Reversible Binding of CO2 via a Dearomatization/Rearomatization Reaction Sequence. Organometallics 2017, 36, 839-848. (b) Filonenko, G. A.; Smykowski, D.; Szyja, B. M.; Li, G.; Szczygiel, J.; Hensen, E. J. M.; Pidko, E. A. Catalytic Hydrogenation of CO₂ to Formates by a Lutidine-Derived Ru-CNC Pincer Complex: Theoretical Insight into the Unrealized Potential. ACS Catal. 2015, 5, 1145-1154. (c) Vogt, M.; Nerush, A.; Diskin-Posner, Y.; Ben-David, Y.; Milstein, D. Reversible CO₂ Binding Triggered by Metal-Ligand Cooperation in a Rhenium(I) PNP Pincer-Type Complex and the Reaction with Dihydrogen. Chem. Sci. 2014, 5, 2043-2051. (d) Huff, C. A.; Kampf, J. W.; Sanford, M. S. Role of a Noninnocent Pincer Ligand in the Activation of CO2 at (PNN)Ru(H)(CO). Organometallics 2012, 31, 4643-4645. (e) Vogt, M.; Gargir, M.; Iron, M. A.; Diskin-Posner, Y.; Ben-David, Y.; Milstein, D. A new mode of activation of CO₂ by metal-ligand cooperation with reversible C-C and M-O bond formation at ambient temperature. Chem. - Eur. J. 2012, 18, 9194-9197. (f) Filonenko, G. A.; Conley, M. P.; Coperet, C.; Lutz, M.; Hensen, E. J. M.; Pidko, E. A. The impact of Metal-Ligand Cooperation in Hydrogenation of Carbon Dioxide Catalyzed by Ruthenium PNP Pincer. ACS Catal. 2013, 3, 2522-2526. (g) Huff, C. A.; Sanford, M. S. Catalytic CO₂ Hydrogenation to Formate by a Ruthenium Pincer Complex. ACS Catal. 2013, 3, 2412-2416. (h) Rivada-Wheelaghan, O.; Dauth, A.; Leitus, G.; Diskin-Posner, Y.; Milstein, D. Synthesis and Reactivity of Iron Complexes with a New Pyrazine-Based Pincer Ligand, and Application in Catalytic Low-Pressure Hydrogenation of Carbon Dioxide. Inorg. Chem. 2015, 54, 4526-4538. (i) Sieh, D.; Lacy, D. C.; Peters, J. C.; Kubiak, C. P. Reduction of CO₂ by Pyridine Monoimine Molybdenum Carbonyl Complexes: Cooperative Metal-Ligand Binding of CO₂. Chem. - Eur. J. 2015, 21, 8497-8503. (j) Zhang, Y.; MacIntosh, A. D.; Wong, J. L.; Bielinski, E. A.; Williard, P. G.; Mercado, B. Q.; Hazari, N.; Bernskoetter, W. H. Iron Catalyzed CO₂ Hydrogenation to Formate Enhanced by Lewis Acid Co-Catalysts. Chem. Sci. 2015, 6, 4291-4299. (k) Feller, M.; Gellrich, U.; Anaby, A.; Diskin-Posner, Y.; Milstein, D. Reductive Cleavage of CO2 by Metal-Ligand-Cooperation Mediated by an Iridium Pincer Complex. I. Am. Chem. Soc. 2016, 138, 6445-6454. (1) Kumar, A.; Daw, P.; Espinosa-Jalapa, N. A.; Leitus, G.; Shimon, L. J. W.; Ben-David, Y.; Milstein, D. CO₂ activation by manganese pincer complexes through different modes of metal-ligand cooperation. Dalton Trans. 2019, 48, 14580-14584. (m) Heuermann, I.; Heitmann, B.; Stichauer, R.;

- Duvinage, D.; Vogt, M. Rh(I) Complex with a Tridentate Pyridine-Amino-Olefin Actor Ligand-Metal-Ligand Cooperative Activation of CO_2 and Phenylisocyanate under C-C and Rh-E (E = O, N) Bond Formation. *Organometallics* **2019**, 38, 1787–1799.
- (4) Stichauer, R.; Vogt, M. Cooperative Binding of SO₂ under M-O and C-S Bond Formation in a Rhenium(I) Complex with Activated Amino- or Iminopyridine Ligand. *Organometallics* **2018**, *37*, 3639–3643.
- (5) (a) Perdriau, S.; Zijlstra, D. S.; Heeres, H. J.; de Vries, J. G.; Otten, E. A Metal-Ligand Cooperative Pathway for Intermolecular Oxa-Michael Additions to Unsaturated Nitriles. *Angew. Chem., Int. Ed.* **2015**, *54*, 4236–4240. (b) Eijsink, L. E.; Perdriau, S. C. P.; de Vries, J. G.; Otten, E. Metal-ligand cooperative activation of nitriles by a ruthenium complex with a de-aromatized PNN pincer ligand. *Dalton Trans.* **2016**, *45*, 16033–16039. (c) Guo, B.; de Vries, J. G.; Otten, E. Hydration of nitriles using a metal-ligand cooperative ruthenium pincer catalyst. *Chem. Sci.* **2019**, *10*, 10647–10652. (d) Vogt, M.; Nerush, A.; Iron, M. A.; Leitus, G.; Diskin-Posner, Y.; Shimon, L. J. W.; Ben-David, Y.; Milstein, D. Activation of Nitriles by Metal Ligand Cooperation. Reversible Formation of Ketimido- and Enamido-Rhenium PNP Pincer Complexes and Relevance to Catalytic Design. *J. Am. Chem. Soc.* **2013**, *135*, 17004–17018.
- (6) (a) Erken, C.; Kaithal, A.; Sen, S.; Weyhermüller, T.; Hölscher, M.; Werlé, C.; Leitner, W. Manganese-catalyzed hydroboration of carbon dioxide and other challenging carbonyl groups. Nat. Commun. 2018, 9, 4521. (b) Takemoto, S.; Ito, T.; Yamazaki, Y.; Tsujita, M.; Matsuzaka, H. Metal-ligand cooperative activation of elementhydrogen bonds (element = C, N, O, Cl, B) on a dinuclear ruthenium bridging imido complex. J. Organomet. Chem. 2016, 812, 158-166. (c) Xu, Y.; Rettenmeier, C. A.; Plundrich, G. T.; Wadepohl, H.; Enders, M.; Gade, L. H. Borane-Bridged Ruthenium Complex Bearing a PNP Ligand: Synthesis and Structural Characterization. Organometallics 2015, 34, 5113-5118. (d) Muller, F.; Trincado, M.; Pribanic, B.; Vogt, M.; Grutzmacher, H. Stable BH3 adducts to rhodium amide bonds. J. Organomet. Chem. 2016, 821, 154-162. (e) Schneck, F.; Assmann, M.; Balmer, M.; Harms, K.; Langer, R. Selective Hydrogenation of Amides to Amines and Alcohols Catalyzed by Improved Iron Pincer Complexes. Organometallics 2016, 35, 1931-1943.
- (7) (a) Praneeth, V. K. K.; Ringenberg, M. R.; Ward, T. R. Redox-Active Ligands in Catalysis. *Angew. Chem., Int. Ed.* **2012**, *51*, 10228–10234. (b) Lyaskovskyy, V.; de Bruin, B. Redox Non-Innocent Ligands: Versatile New Tools to Control Catalytic Reactions. *ACS Catal.* **2012**, *2*, 270–279. (c) Luca, O. R.; Crabtree, R. H. Redox-active ligands in catalysis. *Chem. Soc. Rev.* **2013**, *42*, 1440–1459. (d) van der Vlugt, J. I. Radical-Type Reactivity and Catalysis by Single-Electron Transfer to or from Redox-Active Ligands. *Chem. Eur. J.* **2019**, *25*, 2651–2662. (e) Alig, L.; Fritz, M.; Schneider, S. First-Row Transition Metal (De)Hydrogenation Catalysis Based On Functional Pincer Ligands. *Chem. Rev.* **2019**, *119*, 2681–2751.
- (8) Weinberg, D. R.; Gagliardi, C. J.; Hull, J. F.; Murphy, C. F.; Kent, C. A.; Westlake, B. C.; Paul, A.; Ess, D. H.; McCafferty, D. G.; Meyer, T. J. Proton-Coupled Electron Transfer. *Chem. Rev.* **2012**, *112*, 4016–4093.
- (9) (a) Ringenberg, M. R.; Kokatam, S. L.; Heiden, Z. M.; Rauchfuss, T. B. Redox-Switched Oxidation of Dihydrogen Using a Non-Innocent Ligand. J. Am. Chem. Soc. 2008, 130, 788–789. (b) Schneck, F.; Finger, M.; Tromp, M.; Schneider, S. Chemical Non-Innocence of an Aliphatic PNP Pincer Ligand. Chem. Eur. J. 2017, 23, 33–37. (c) Rosenkoetter, K. E.; Wojnar, M. K.; Charette, B. J.; Ziller, J. W.; Heyduk, A. F. Hydrogen-Atom Noninnocence of a Tridentate [SNS] Pincer Ligand. Inorg. Chem. 2018, 57, 9728–9737. (d) Vaddypally, S.; Tomlinson, W.; O'Sullivan, O. T.; Ding, R.; Van Vliet, M. M.; Wayland, B. B.; Hooper, J. P.; Zdilla, M. J. Activation of C-H, N-H, and O-H Bonds via Proton-Coupled Electron Transfer to a Mn(III) Complex of Redox-Noninnocent Octaazacyclotetradecadiene, a Catenated-Nitrogen Macrocyclic Ligand. J. Am. Chem. Soc. 2019, 141, 5699–5709. (e) McManus, C.; Mondal, P.; Lovisari, M.; Twamley, B.; McDonald, A. R. Carboxamidate Ligand Noninnocence

- in Proton Coupled Electron Transfer. Inorg. Chem. 2019, 58, 4515-4523. (f) Deibel, N.; Hohloch, S.; Schweinfurth, D.; Weisser, F.; Grupp, A.; Sarkar, B. Three-Way Cooperativity in d⁸ Metal Complexes with Ligands Displaying Chemical and Redox Non-Innocence. Chem. - Eur. J. 2014, 20, 15178-15187. (g) Lindley, B. M.; Bruch, Q. J.; White, P. S.; Hasanayn, F.; Miller, A. J. M. Ammonia Synthesis from a Pincer Ruthenium Nitride via Metal-Ligand Cooperative Proton-Coupled Electron Transfer. J. Am. Chem. Soc. 2017, 139, 5305-5308. (h) Margulieux, G. W.; Bezdek, M. J.; Turner, Z. R.; Chirik, P. J. Ammonia Activation, H2 Evolution and Nitride Formation from a Molybdenum Complex with a Chemically and Redox Noninnocent Ligand. J. Am. Chem. Soc. 2017, 139, 6110-6113. (i) Luo, G.-G.; Zhang, H.-L.; Tao, Y.-W.; Wu, Q.-Y.; Tian, D.; Zhang, Q. Recent progress in ligand-centered homogeneous electrocatalysts for hydrogen evolution reaction. Inorg. Chem. Front. 2019, 6, 343-354.
- (10) Cronin, S. P.; Strain, J. M.; Mashuta, M. S.; Spurgeon, J. M.; Buchanan, R. M.; Grapperhaus, C. A. Exploiting Metal-Ligand Cooperativity to Sequester, Activate, and Reduce Atmospheric Carbon Dioxide with a Neutral Zinc Complex. *Inorg. Chem.* **2020**, *59*, 4835.
- (11) Durgaprasad, G.; Luna, J. A.; Spielvogel, K. D.; Haas, C.; Shaw, S. K.; Daly, S. R. Ru(II) Complexes with a Chemical and Redox-Active S_2N_2 Ligand: Structures, Electrochemistry, and Metal-Ligand Cooperativity. *Organometallics* **2017**, *36*, 4020–4031.
- (12) Spielvogel, K. D.; Coughlin, E. J.; Petras, H.; Luna, J. A.; Benson, A.; Donahue, C. M.; Kibasa, A.; Lee, K.; Salacinski, R.; Bart, S. C.; Shaw, S. K.; Shepherd, J. J.; Daly, S. R. The Influence of Redox-Innocent Donor Groups in Tetradentate Ligands Derived from o-Phenylenediamine: Electronic Structure Investigations with Nickel. *Inorg. Chem.* **2019**, *58*, 12756–12774.
- (13) We are using $I_{\rm pc}/I_{\rm pa}$ as the metric for electrochemical reversibility. The ΔE peak values are relatively large, which is commensurate with significant uncompensated resistance and is common for CV measurements in organic solvents.
- (14) An irreversible feature is also observed at -2.48 V when scanning the full solvent window.
- (15) The tentative CV assignments made previously for 1 were incorrect and are revised here; see ref 11.
- (16) Potter, R. G.; Camaioni, D. M.; Vasiliu, M.; Dixon, D. A. Thermochemistry of Lewis Adducts of BH₃ and Nucleophilic Substitution of Triethylamine on NH₃BH₃ in Tetrahydrofuran. *Inorg. Chem.* **2010**, *49*, 10512–10521.
- (17) Khan, M. M. T.; Srinivas, D.; Kureshy, R. I.; Khan, N. H. Synthesis, characterization, and EPR studies of stable ruthenium(III) Schiff base chloro and carbonyl complexes. *Inorg. Chem.* **1990**, *29*, 2320–2326.
- (18) Chatterjee, M.; Mondal, S.; Ghosh, P.; Kaim, W.; Lahiri, G. K. Mononuclear and Dinuclear Ruthenium Complexes of cis- and trans-Thioindigo: Geometrical and Electronic Structure Analyses. *Inorg. Chem.* **2018**, *57*, 12187–12194.
- (19) This generation and cooperative capture of BH₂ is reminiscent of that reported recently for a molybdenum thiolate complex. See Hou, S.-F.; Chen, J.-Y.; Xue, M.; Jia, M.; Zhai, X.; Liao, R.-Z.; Tung, C.-H.; Wang, W. ACS Catal. 2020, 10, 380–390.
- (20) (a) Green, I. G.; Roberts, B. P. Homolytic reactions of ligated boranes. Part 3. Electron spin resonance studies of radicals derived from dialkylamine-boranes. *J. Chem. Soc., Perkin Trans.* 2 1986, 1597–1606. (b) Kirwan, J. N.; Roberts, B. P. Homolytic reactions of ligated boranes. Part 11. Electron spin resonance studies of radicals derived from primary amine-boranes. *J. Chem. Soc., Perkin Trans.* 2 1989, 539–550.
- (21) Metters, O. J.; Chapman, A. M.; Robertson, A. P. M.; Woodall, C. H.; Gates, P. J.; Wass, D. F.; Manners, I. Generation of aminoborane monomers RR'N = BH₂ from amine-boronium cations [RR'NH-BH₂L]⁺: metal catalyst-free formation of polyaminoboranes at ambient temperature. *Chem. Commun.* **2014**, *50*, 12146–12149.
- (22) (a) Lee, C.; Yang, W.; Parr, R. G. Development of the Colle-Salvetti correlation-energy formula into a functional of the electron

density. *Phys. Rev. B: Condens. Matter Mater. Phys.* **1988**, 37, 785–789. (b) Becke, A. D. Density-functional thermochemistry. III. The role of exact exchange. *J. Chem. Phys.* **1993**, 98, 5648–5652. (c) Grimme, S.; Antony, J.; Ehrlich, S.; Krieg, H. A consistent and accurate ab initio parametrization of density functional dispersion correction (DFT-D) for the 94 elements H-Pu. *J. Chem. Phys.* **2010**, *132*, 154104.

(23) Frisch, M. J.; Trucks, G. W.; Schlegel, H. B.; Scuseria, G. E.; Robb, M. A.; Cheeseman, J. R.; Scalmani, G.; Barone, V.; Mennucci, B.; Petersson, G. A.; Nakatsuji, H.; Caricato, M.; Li, X.; Hratchian, H. P.; Izmaylov, A. F.; Bloino, J.; Zheng, G.; Sonnenberg, J. L.; Hada, M.; Ehara, M.; Toyota, K.; Fukuda, R.; Hasegawa, J.; Ishida, M.; Nakajima, T.; Honda, Y.; Kitao, O.; Nakai, H.; Vreven, T.; Montgomery, J. A., Jr.; Peralta, J. E.; Ogliaro, F.; Bearpark, M.; Heyd, J. J.; Brothers, E.; Kudin, K. N.; Staroverov, V. N.; Kobayashi, R.; Normand, J.; Raghavachari, K.; Rendell, A.; Burant, J. C.; Iyengar, S. S.; Tomasi, J.; Cossi, M.; Rega, N.; Millam, J. M.; Klene, M.; Knox, J. E.; Cross, J. B.; Bakken, V.; Adamo, C.; Jaramillo, J.; Gomperts, R.; Stratmann, R. E.; Yazyev, O.; Austin, A. J.; Cammi, R.; Pomelli, C.; Ochterski, J. W.; Martin, R. L.; Morokuma, K.; Zakrzewski, V. G.; Voth, G. A.; Salvador, P.; Dannenberg, J. J.; Dapprich, S.; Daniels, A. D.; Farkas, O.; Foresman, J. B.; Ortiz, J. V.; Cioslowski, J.; Fox, D. J. Gaussian 09, revision B.01; Gaussian, Inc.: Wallingford, CT, 2009.

(24) As is typical with the B3LYP functional, some of the calculated bond distances are slightly overestimated. See Tables S4 and S5.

NOTE ADDED AFTER ASAP PUBLICATION

This paper was published July 8, 2020, with a former production version of the abstract image. The corrected version was posted on July 10, 2020.